ACS APPLIED MATERIALS & INTERFACES

Research Article

www.acsami.org

Reductant and Sequence Effects on the Morphology and Catalytic Activity of Peptide-Capped Au Nanoparticles

Beverly D. Briggs,[†] Yue Li,[‡] Mark T. Swihart,[‡] and Marc R. Knecht*,[†]

[†]Department of Chemistry, University of Miami, 1301 Memorial Drive, Coral Gables, Florida 33146, United States

[‡]Department of Chemical and Biological Engineering, University at Buffalo (SUNY), Buffalo, New York 14260, United States

Supporting Information

ABSTRACT: The use of peptides as capping ligands for materials synthesis has been widely explored. The ambient conditions of bio-inspired syntheses using molecules such as peptides represent an attractive route for controlling the morphology and activity of nanomaterials. Although various reductants can be used in such syntheses, no comprehensive comparison of the same bio-based ligand with different reductants has been reported. In this contribution, peptides AuBP1, AuBP2, and Pd4 are used in the synthesis of Au nanoparticles. The reductant strength is varied by using three different reducing agents: $NaBH_4$, hydrazine, and ascorbic acid. These changes in reductant produce significant morphological differences in the final particles. The weakest reductant, ascorbic acid, yields large, globular nanoparticles with rough surfaces, whereas the strongest reductant, $NaBH_4$, yields small, spherical, smooth nanomaterials. Studies of 4-nitrophenol reduction using the Au nanoparticles as catalysts reveal a decrease in activation energy for the large, globular, rough materials relative to the small, spherical, smooth materials. These studies demonstrate that modifying the reductant is a simple way to control the activity of peptide-capped nanoparticles.

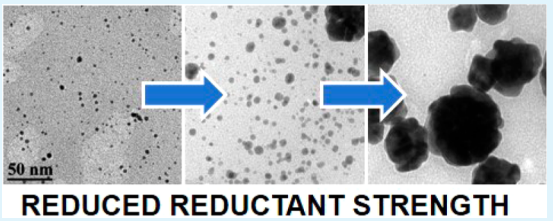

KEYWORDS: *Au nanoparticles, peptides, bio-inspired synthesis, reductant, catalysis*

INTRODUCTION

Bio-inspired strategies for producing inorganic nanoparticles (NP) are of great interest because they can control the structure of the material under very mild synthetic conditions.[1,2] Biomolecule-capped nanomaterials have proven useful in many applications, including catalysis, biosensing, and NP assembly, where the biotic interface can play an integral role in their performance. Many biological entities have been used to passivate NP surfaces, including DNA,[3−6] viruses,[7] and peptides.[8−14] Peptides are particularly promising, because they can provide biomolecular recognition for specific binding to metal interfaces and they are relatively easy to prepare. Biocombinatorial selection methods such as phage and cell-surface display have been used to isolate many peptides with affinity for metal,[12,15] metal oxide,[8,16] and metal sulfide surfaces,[17,18] with selectivity for specific target materials.[19,20]

Although NPs of many compositions have been prepared using peptides, Au NPs are of particular interest due to their applications in sensing,[21] catalysis,[22−24] diagnostics,[25] and bionanocombinatorics.[19,20,26] A key property of Au NPs is their localized surface plasmon resonance (LSPR), which produces strong scattering and absorption of light over a wavelength range that can be tuned by varying the NP size and shape.[27] Peptides can provide control over morphology and activity of Au NPs through their sequence specific interactions with the Au surface.[23] The AuBP1 (WAGAKRLVLRRE) and AuBP2 (WALRRSIRRQSY) sequences are exemplar peptides with affinity for Au and the ability to generate nearly monodisperse NPs.[11,23] Sarikaya and colleagues isolated these peptides via phage display and demonstrated that the biomolecular structure (linear vs cyclic) played a critical role in controlling the overall affinity of the sequence for the metal surface.[11] More recently, Tang et al. demonstrated the importance of the nature of binding to the metal surface, which can be predominantly enthalpic or entropic.[19] Both AuBP1 and AuBP2 were classified as enthalpic binders, meaning that they incorporate several residues throughout the sequence that anchor the biomolecule to the metallic surface in a small number of possible configurations.[19] Specifically, AuBP1 and AuBP2 each have four anchor residues dispersed throughout the sequence (Trp-1, Arg-6, Arg-10, and Arg-11 in AuBP1, Trp-1, Arg-4, Arg-5, and Tyr-12 in AuBP2).[19] Conversely, a peptide exhibiting entropically driven binding has fewer anchor residues, but assumes many different surface bound conformations, which imbue it with relatively high entropy in the bound state. The Pd4 peptide (TSNAVHPTLRHL), originally isolated with affinity for palladium (Pd), is an exemplar of entropic binding peptides on Au.[28] It includes only two anchor residues (His-6 and His-11); however, extensive simulation studies revealed a relatively large number of binding conformations for the peptide on an aqueous Au surface.[19] Peptide-capped Au NPs prepared using

Received: February 13, 2015
Accepted: April 3, 2015
Published: April 3, 2015

DOI: 10.1021/acsami.5b01461
ACS Appl. Mater. Interfaces 2015, 7, 8843−8851

$NaBH_4$ as the reductant with each of these peptides were spherical, and their size was correlated with the number of anchor residues (i.e., enthalpic contribution), rather than the overall binding affinity, which is related to the free energy change of binding.[23]

Beyond the peptide−metal interactions, several other factors control the growth and final structure of peptide-capped Au NPs.[29−31] NP formation is initiated by addition of a reductant that reduces dissolved Au^{3+} to insoluble Au^0, initiating NP nucleation and growth. Previous studies have shown that altering the strength of the reductant changes the rate of reduction, producing changes in NP size.[31] Thus, different reductants produce NPs with different LSPR spectra, catalytic activities, and other properties that depend upon the NP size and shape.[29−31] A strong reductant drives a burst of nucleation due to the high concentration of Au^0 produced by rapid reduction. The high nucleation density produces smaller final NPs as a fixed amount of Au precursor deposits onto a larger number of nuclei. A weaker reductant produces a lower concentration of Au^0 through slower reduction. This results in a lower probability of overcoming the barrier to nucleation, and therefore a lower nucleation density. Ultimately, this produces a smaller number of larger particles.[32] Most prior studies of these effects employed standard NP surface passivants, such as thiols on Au, and produced quasi-spherical NPs regardless of the reductant employed.[33] The effects of peptide on NP generation with different reductants have not been systematically studied. The kinetics and thermodynamics of binding of biomolecules with the Au surface are significantly more complex than those of thiols and similar passivants. As discussed above, sequence-dependent interactions at the NP surface control the peptide binding and therefore the peptide's role in arresting particle growth.[34] If understood, this can provide enhanced control over particle size, morphology, surface structure, and properties that remain difficult to achieve via traditional approaches.

One area of rapidly growing interest for Au NPs is catalysis. The reduction of 4-nitrophenol is widely employed as a probe reaction for evaluating the catalytic activity of such materials.[23,35−40] The substrate, 4-nitrophenol, is a known pollutant and toxin that can be easily reduced to 4-aminophenol, a major pharmaceutical precursor.[40] This reaction is relatively simple and can be easily monitored using UV−vis spectroscopy in aqueous solutions at ambient temperature.[37,40] Importantly, the reduction of 4-nitrophenol is known to occur via a surface reaction mechanism in which adsorption of hydrogen and the substrate to the metal surface is required for catalytic turnover.[36] This is advantageous for the peptide-capped NPs in that it provides a direct measure of the accessibility of the metal surface that cannot be readily assessed by other methods.

Here we study the combined effects of reductant strength and peptide binding at the Au NP interface based upon the rate of NP nucleation and growth, and the catalytic properties of the final materials. Au NPs were generated using three different peptides, AuBP1, AuBP2, and Pd4, which span a known range of binding affinity and balance between enthalpic and entropic binding character.[19] Each of these was used in combination with three different reductants: sodium borohydride ($NaBH_4$), hydrazine, and ascorbic acid. The product NPs were fully characterized using UV−vis absorbance spectroscopy, transmission electron microscopy (TEM), and selected area electron diffraction (SAED) analysis. Their catalytic activity for the reduction of 4-nitrophenol to 4-aminophenol was also quantified. The results and synthetic strategies provide a path toward realizing low temperature and facile mechanisms of tuning Au NP size, shape, and surface state for applications in biosensing, catalysis, and related fields.

EXPERIMENTAL SECTION

Materials. $HAuCl_4$ was purchased from Acros Organics, whereas $NaBH_4$ and hydrazine monohydrate were acquired from Sigma-Aldrich. Trifluoroacetic acid (TFA), tri-isopropyl silane (TIS), and 4-nitrophenol were obtained from Alfa Aesar, and ascorbic acid, acetonitrile, methanol, and *N*,*N*-dimethylformamide were purchased from BDH Chemicals. Finally, all FMOC-protected amino acids, Wang resins, and coupling reagents were acquired from Advanced Chemtech. Ultrapure water (18.2 MΩ·cm) was used for all experiments and all reagents were used as received.

Peptide Synthesis. Standard solid-phase peptide synthesis protocols were used with a TETRAS peptide synthesizer (Creosalus).[41] Peptides were cleaved from the Wang resins using a TIS/H_2O/TFA cleavage cocktail and purified using reverse-phase high performance liquid chromatography (HPLC). The purified peptide sequences were confirmed using matrix-assisted laser desorption/ionization time-of-flight (MALDI-TOF) mass spectrometry.

Nanoparticle Synthesis. Au NPs were prepared by minor modifications of previously described methods.[23] Modifications to the synthesis protocol using the different reductants (ascorbic acid and hydrazine in place of the $NaBH_4$ used previously) are discussed below. Briefly, 0.50 mL of a 1.0 mM peptide solution was diluted with 4.46 mL of H_2O in a glass vial. To this was added 0.01 mL of 100 mM $HAuCl_4$, and the solution was mixed vigorously for 15 min. Next, 0.03 mL of freshly prepared 100 mM $NaBH_4$ was added and the solution was mixed again. This provides a 3-fold molar excess of $NaBH_4$ compared to Au. The NPs were allowed to reduce for 60 min prior to analysis or use. Identical synthetic protocols were employed using the other reductants, with a 3-fold molar excess of ascorbic acid to Au^{3+} or a 2-fold molar excess of hydrazine.

Characterization. TEM analysis was done using a JEOL JEM-2010 microscope operating at 200 kV. The samples were prepared by drop-casting 5 μL of the NP solution onto a carbon-coated 400 mesh Cu grid (EM Sciences), which was allowed to dry overnight. UV−vis monitoring of NP formation, as well as the reduction of 4-nitrophenol, was conducted using an Agilent 8453 spectrometer. Samples were analyzed using a quartz cuvette with a 1 cm optical path length.

4-Nitrophenol Reduction Reaction. The catalytic activity of the Au NPs was evaluated using the reduction of 4-nitrophenol to 4-aminophenol following previously established protocols.[37,42] In a 1 cm quartz cuvette (nominal volume = 3.5 mL), 1.0 mL of the Au NP solution was combined with 1.0 mL of freshly prepared 15 mM $NaBH_4$ in water. Next, 1.0 mL of a 150 μM 4-nitrophenol solution, prepared in water, was added to initiate the reaction. Monitoring of the change in the absorbance at 400 nm at 20.0 s intervals for 12.0 min was conducted in triplicate at 20−50 °C for all nine material sets (Au NPs prepared using each of the three peptides, reduced using each of the three reductants).

RESULTS AND DISCUSSION

Nanoparticle Synthesis and Characterization. Au NPs were prepared using three peptides: AuBP1, AuBP2, and Pd4. These sequences were selected to span a known range of binding parameters for Au. AuBP1 and AuBP2, specifically identified for their affinity to bind Au surfaces,[11] have binding affinities (ΔG of binding) on Au of −37.6 ± 0.9 and −36.4 ± 0.3 kJ/mol, respectively.[19] Pd4 was originally isolated via phage display for the ability to bind Pd. It binds to Au with a ΔG value of −30.3 ± 0.2 kJ/mol,[19] which is smaller than its binding affinity for Pd (−33.0 ± 0.5 kJ/mol).[19,28,43] In addition, these three peptides have differing thermodynamic driving forces for binding to the Au surface. In this regard, both the AuBP1 and AuBP2 have several anchor residues interspersed throughout

DOI: 10.1021/acsami.5b01461
ACS Appl. Mater. Interfaces 2015, 7, 8843−8851

the sequence, thus they have been classified as enthalpic binding peptides. Conversely, the Pd4 only has two anchors at the histidines; however, it can adopt many different conformations on the Au surface, and is thus classified as an entropic binder. Taken together, these three peptides provide different binding parameters (both in overall affinity and thermodynamic driving forces), spanning a significant range of possible interactions.

For nanoparticle synthesis experiments, each peptide was mixed with Au^{3+} in water at a Au:peptide ratio of 2:1 for 15 min prior to reduction. This allows for complexation of the metal ions to the biomolecule. After complexation, each solution was reduced separately with one of three reductants: $NaBH_4$, hydrazine, or ascorbic acid. These were selected to span a range of strengths of reducing agents. $NaBH_4$ is the strongest reductant in this set, followed by hydrazine, with ascorbic acid being the weakest reductant.[44,45] For both $NaBH_4$ and ascorbic acid, a 3-fold molar excess relative to Au^{3+} was employed; however, a 2-fold molar excess of hydrazine was used. The lower ratio of hydrazine to Au was specifically chosen as this was the ratio used in previous studies.[46] In all cases, an obvious color change was noted upon reduction, as described below, and the product NP dispersions remained stable for >24 h without any visible precipitation.

Initial characterization of the NP formation process as a function of both the peptide and reductant was completed using UV−vis spectroscopy (Figure 1). For each system, the

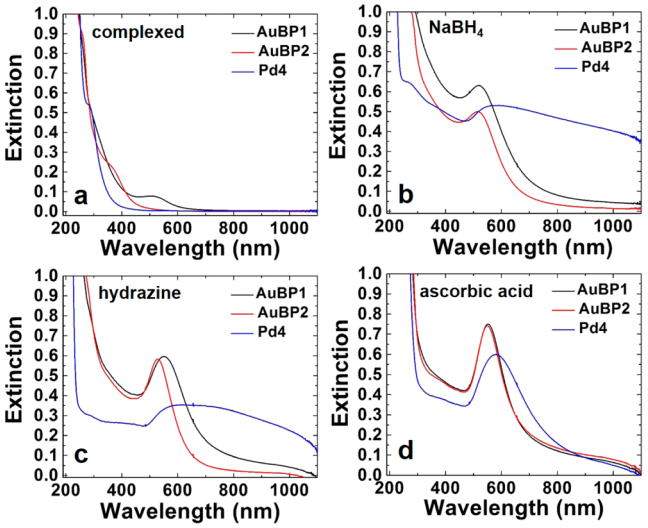

Figure 1. UV−vis analysis of Au NP formation. Panel a presents the spectra of each Au^{3+}/peptide complex prior to reduction, whereas panels b−d show the materials after reduction with (b) $NaBH_4$, (c) hydrazine, and (d) ascorbic acid.

spectra were background corrected using the peptide solution at the reaction concentration, thus the observed absorbance arises only from the Au^{3+}/peptide complex and/or the NPs. As shown in Figure 1a, for the AuBP1-system prior to reduction, a minor peak at 500 nm was visible, whereas a shoulder absorbance is visible at ~400 nm for the AuBP2-mediated reaction. For the Pd4-based system, no significant peaks were visible in the spectrum. Upon reduction, an absorbance peak associated with the Au NP LSPR was evident, with a peak position and shape that varied with both the peptide and reductant. For $NaBH_4$ specifically (Figure 1b), when AuBP1 and AuBP2 were used to cap the Au NPs, a distinct and relatively sharp LSPR was observed at 520 nm; however, when Pd4 was used to generate the Au NPs, a broader and red shifted LSPR absorbance was observed. This suggests that the Pd4-capped Au NPs are larger, more polydisperse, and/or more aggregated in solution than the AuBP1- and AuBP2-capped materials. With hydrazine as the reductant (Figure 1c), the AuBP1- and AuBP2-capped materials again have a distinct LSPR absorbance after reduction. In this system, the peak position is slightly red shifted, compared to the NPs produced with $NaBH_4$, to 550 nm for the AuBP1-capped materials and 530 nm for the AuBP2-capped structures. Interestingly, for the hydrazine reductant, the AuBP1-capped NPs resulted in a broader LSPR absorbance as compared to the AuBP2 materials. For the Au NPs capped with Pd4 and reduced with hydrazine, a broad absorbance with a peak beginning at 580 nm was again observed. Finally, when ascorbic acid was used as the reductant (Figure 1d), the results were substantially different. The spectra for the AuBP1- and AuBP2-capped materials were nearly identical with a distinct plasmon band at 550 nm. This was the sharpest LSPR observed among all of the samples. For the Pd4-capped materials reduced with ascorbic acid, a distinct LSPR peak at 580 nm was noted that was significantly sharper than that observed for the Pd4-capped NPs prepared using the stronger reducing agents.

TEM imaging and analysis to extract nanoparticle size information on all materials was carried out to directly observe the NP morphology changes with variations in reductant and capping peptide (Figure 2). For the sizing analysis, >100 NPs were counted from at least three separate TEM images to generate particle size histograms (Supporting Information, Figure S1). SAED analysis of all of the prepared Au NPs was conducted (Supporting Information, Figure S2), and in all cases

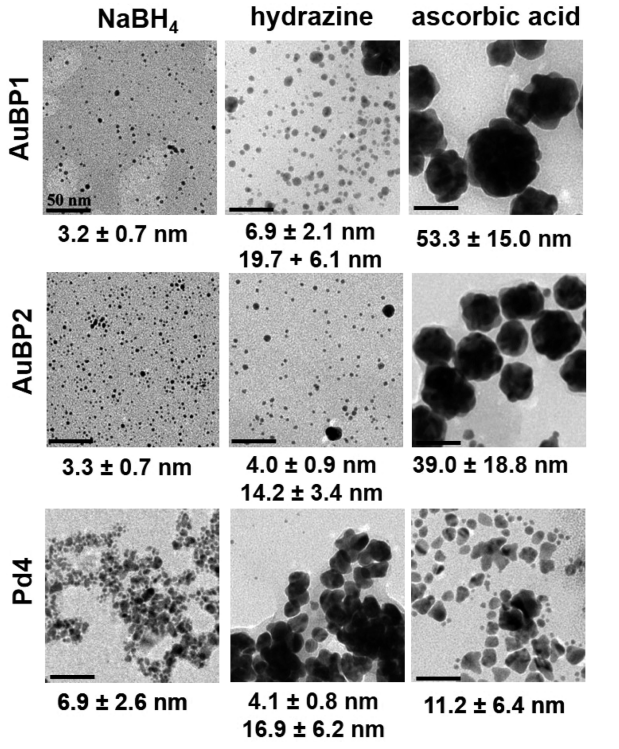

Figure 2. TEM images of the Au NPs prepared as a function of peptide passivant and reductant. All scale bars are 50 nm.

DOI: 10.1021/acsami.5b01461
ACS Appl. Mater. Interfaces 2015, 7, 8843−8851

only diffraction rings corresponding to Au were visible. Particles produced using $NaBH_4$ as the reducing agent gave SAED patterns with more diffuse rings, consistent with smaller particle size, whereas those produced using ascorbic acid gave the sharpest rings, with discrete spots associated with individual crystallites. Using the AuBP1 and AuBP2 peptides as the capping agents with $NaBH_4$ as the reductant yielded small, quasi-spherical Au NPs with average diameters (±1 standard deviation) of 3.2 ± 0.7 and 3.3 ± 0.7 nm, respectively. Using the Pd4 peptide to stabilize the particles under the same conditions, more polydisperse NPs with an average diameter of 6.9 ± 2.6 nm were obtained. These results are consistent with the UV−vis spectra of the materials, in which the AuBP1 and AuBP2 systems displayed sharp LSPR bands, whereas a broader, red shifted LSPR peak was observed for the Pd4-based structures. However, the very broad LSPR peak from the materials prepared using the Pd4 cannot be accounted for based on the increased size and polydispersity alone. This suggests that the Pd4-capped particles are significantly aggregated in solution, even though they do not aggregate to an extent that they visibly precipitate. With hydrazine as the reductant in combination with each of the three peptides, a bimodal NP size distribution was observed. Specifically, for AuBP1, spherical particles were again noted, but with a larger average diameter of 6.9 ± 2.1 nm (88% of the sample, by number). These were accompanied by larger agglomerates with a diameter of 19.7 ± 6.1 nm (12% of the sample, by number). For the AuBP2-capped NPs reduced with hydrazine, the results were similar to the smaller NPs (4.0 ± 0.9 nm) comprising 91% of the population and the larger agglomerates (14.2 ± 3.4 nm) accounting for 9% of the sample. Finally, for the materials fabricated using the Pd4 peptide with hydrazine, the bimodal trend was continued with small NPs of 4.1 ± 0.8 nm diameter comprising 71% of the sample and larger NPs of 16.9 ± 6.2 nm diameter comprising 29%. Interestingly, the Pd4-capped system yielded a greater percentage of larger NPs as well as a greater occurrence of aggregation, as noted via TEM imaging. These results are again consistent with the UV−vis spectra of the materials. In this regard, the AuBP1- and AuBP2-capped materials reduced with hydrazine displayed red shifted and broadened LSPRs as compared to the comparable structures reduced with $NaBH_4$. This is a direct consequence of the increase in particle size and inclusion of significantly larger particles. Furthermore, the AuBP1-capped particles were generally larger and more polydisperse in size, giving rise the broadened and red shifted LSPR relative to the AuBP2-based materials. Finally, the Pd4-capped structures again appeared to be aggregated and nonspherical in shape, generating the very broad LSPR absorbance.

TEM imaging of Au NPs prepared using ascorbic acid showed dramatic differences in particle size and morphology compared to NPs prepared using the stronger reductants. The AuBP1-capped NPs produced using ascorbic acid had an average diameter of 53.3 ± 15.0 nm. More interestingly, the surface structure of these materials was quite rough. Similar nanomaterials were prepared using AuBP2 and ascorbic acid, but the average diameter of these globular NPs was 39.0 ± 18.8 nm. Interestingly, when Pd4 was used with ascorbic acid, smaller irregularly shaped nanostructures were generated. Their size, as measured along their longest axis, was 11.2 ± 6.4 nm.

For all of the particles produced using AuBP1 and AuBP2, the measured absorbance spectra are consistent with computed spectra based upon the size distributions measured by TEM. Extinction spectra (Supporting Information, Figure S4) were computed via Mie theory assuming spherical particles with a Gaussian size distribution and the mean diameter and standard deviation of diameter obtained from TEM imaging. For the particles reduced with hydrazine, where a bimodal size distribution was observed, only the large particle mode was considered. Because of the strong size-dependence of absorbance and scattering in this size range, the larger subpopulation of particles will dominate the extinction spectrum. The relatively weak LSPR predicted and observed for the $NaBH_4$-reduced particles is associated with their small size and resulting increased damping of the LSPR by interface scattering of electrons. The largest particles, produced using ascorbic acid as the reductant, have the sharpest LSPR peak, which is slightly red-shifted from the peak computed and observed for the hydrazine-reduced particles, due to their larger size. The LSPR spectra observed for the Pd4-capped particles cannot be explained based on the size-distribution of the primary particles, leading us to conclude that they are somewhat aggregated in solution, with a broad range of aggregate sizes, during the absorbance measurement.

The above results illustrate that changes in the peptide and in the reducing agent used in the synthesis can have dramatic and nonobvious effects on the size, shape, and optical properties of the product Au NPs. The binding at the metal NP interface in solution, as controlled via the peptide sequence, as well as the strength of the reductant each play a significant role in controlling the particle size and morphology. Clearly, these effects do not operate independently, but synergistically. We do not observe universal trends with respect to either the peptide or reductant. For example, for AuBP1 and AuBP2, it can be seen that using a stronger reductant produces smaller NPs, which can be understood based upon the stronger reductant generating a larger number of nuclei via faster reduction of Au^{3+} to Au^0. However, this trend does not hold for the Pd4-capped particles. Similarly, one might expect Pd4 to produce larger particles than AuBP1 and AuBP2, because it has both lower enthalpy and free energy of binding, i.e., it is both a relatively weak binder and an entropically driven binder on Au, but this only proves to be the case for the strongest reducing agent, $NaBH_4$. For weaker reducing agents, the situation is more complex, with the interplay between the biomolecular binding and the reduction kinetics working together to control the final NP structure.

Based upon the UV−vis and TEM results, both the peptide sequence and the reductant play critical roles in controlling the size and morphology of the Au NPs. With respect to the reductant, the rate of the reduction of Au^{3+} to Au^0 is likely to play a central role, as it directly affects the particle nucleation and growth rate. The rate of reduction and of particle formation can be monitored by observing the appearance of the LSPR band for Au NPs. Assuming pseudo-first-order kinetics allows us to extract a rate constant representative of the reduction and particle nucleation and growth process. To this end, the LSPR absorbance was monitored using UV−vis by taking one spectrum per second for the first 5.0 min after addition of the reductant. From this, the rate constant (k) for NP growth can be determined, as presented in Figure 3 for the reactions employing hydrazine and ascorbic acid. Unfortunately, the rate of particle growth using $NaBH_4$ was too rapid to quantify with this approach. Using hydrazine as a reductant, the fastest formation of Au NPs occurred in the presence of the Pd4 peptide (0.0816 ± 0.0120 s^{-1}). For the AuBP1 and AuBP2

DOI: 10.1021/acsami.5b01461
ACS Appl. Mater. Interfaces 2015, 7, 8843−8851

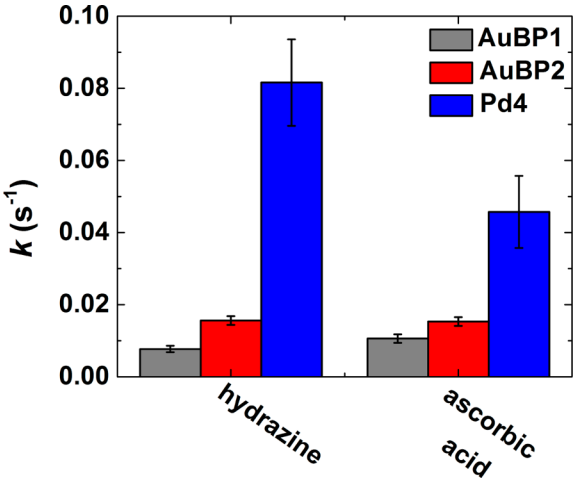

Figure 3. Comparison of the rate of Au NP formation as measured via the growth of the plasmon band. Values could not be determined for the particles reduced using $NaBH_4$ due to their rapid rate of formation.

peptides, which have both greater affinity for Au and more enthalpic binding character, smaller k values were observed: 0.0077 ± 0009 and 0.0156 ± 0.0012 s^{-1}, respectively. The same trend was noted for the weaker ascorbic acid reductant. Faster NP growth was evident using Pd4 (k value = 0.0457 ± 0.0100 s^{-1}), whereas slower NP growth occurred in the presence of AuBP1 (0.0153 ± 0.0012 s^{-1}) and AuBP2 (0.0106 ± 0.0012 s^{-1}) materials. Here, the binding affinity of different peptides for the Au surface varies as AuBP1 > AuBP2 ≫ Pd4,[19] which correlates directly with the trend in observed particle growth rate.

Taken together, the UV−vis and TEM results provide insight into the effects of both the peptide capping agent and reductant upon the final particle morphology. The final morphology depends strongly upon the rate of reduction, which affects particle nucleation and growth rates. The strongest reductant, $NaBH_4$, drives extremely rapid NP nucleation. This high nucleation density gives rise to the smallest particles observed by TEM. This is consistent with the sharp plasmon bands at the shortest wavelengths (520 nm) observed for the NPs produced using $NaBH_4$ with the AuBP1 and AuBP2 peptides. Use of the Pd4 peptide with $NaBH_4$ produced more polydisperse NPs with a broad absorbance spectrum. This can be rationalized based on a high nucleation density coupled with incomplete surface capping that allows the initial NPs to aggregate. With hydrazine, a weaker reducing agent than $NaBH_4$, slower NP nucleation and growth was observed. The lower nucleation density produced by slower reduction ultimately generates larger primary particles. The influence of the affinity of the peptide for the metal surface was more significant in this case. The NPs prepared using hydrazine with any of the peptides were slightly larger than those fabricated using $NaBH_4$, leading to slightly red shifted SPR bands in the UV−vis analysis. Note that the reduction with hydrazine in the presence of Pd4 is substantially faster than in the presence of AuBP1 or AuBP2 (Figure 3). Most interestingly, when the weakest reductant, ascorbic acid, was used, the NP morphology changed substantially. When ascorbic acid was used with AuBP1 or AuBP2, larger NPs with rough surfaces were obtained. These structures presented SPR bands furthest shifted to the red due to their large size. This can be rationalized based on a combination of slow reduction, limited aggregation of primary particles, and slow overgrowth on these aggregates as Au reduction continues. In contrast, when ascorbic acid is used with Pd4, the reduction is faster and more polydisperse, irregular NPs result. Calculation of the anticipated UV−vis spectra for these materials correlated directly to the observed spectroscopic results based upon the size and morphology of the NPs.

The rate of NP nucleation and growth, as measured by the growth of the LSPR absorbance, is directly correlated with the binding affinity of the peptide to the Au surface. For the strongest reductant ($NaBH_4$), the growth rates were too fast to monitor, and the effect of the peptide was limited. For the weaker reductants, the peptides may weakly interact with the growing NP surface in solution throughout the entire process. They can slow growth by complexing with the Au^{3+} ions, reducing the rate of Au^{3+} to Au^0 reduction, and also by adsorbing to the NP surface, slowing deposition of Au^0. The latter mechanism would be affected significantly by the affinity of the peptide for the metal surface, as well as the morphology of the NP interface, as those with the strongest affinity or highest number of anchor residues would more effectively inhibit metal atom deposition compared to peptides that are less strongly bound or whose binding is more entropically driven. This is consistent with the observed rates of particle growth, which for a given reductant were much slower for the relatively strong enthalpically driven binders, AuBP1 and AuBP2, compared to the weaker, entropically driven binder, Pd4. The final particle size, however, is determined by both the growth rate and the nucleation density, and therefore slower growth does not necessarily correlate with smaller final particles.

As a control study, TEM imaging of the AuBP1- and AuBP2-complexes with Au^{3+} ions prior to reduction were acquired. Such studies were completed as minor absorbances were noted in the spectra of these materials, suggesting some reduction to Au^0 may have occurred. In this analysis, the formation of large, branched Au materials were observed with diameters >300 nm (Supporting Information, Figure S3). SAED analysis confirmed that the materials were polycrystalline Au. Additional studies are required to fully understand this unique phenomena.

Based upon the binding mechanism of these peptides on Au,[19] the biomolecules are expected to noncovalently interact with the metallic surface via multiple points of contact, generating a biotic/abiotic interface that maintains the colloidal stability of the NPs. From previous measurements,[11,19] the affinity of the biomolecules (i.e., their overall Gibbs free energy, ΔG, of binding) on Au is similar to that of standard monodentate thiols.[11] However, thiol ligands are covalently attached to the metal interface at a single point, forming a comparatively rigid inorganic/organic interface. Ligands stabilize NP colloids either through steric or electrostatic effects, or a combination of both,[47] depending upon the combination of ligand and solvent. Because the conformational flexibility of the bound peptides is significantly larger than that of the rigidly bound thiols, entropic effects play a more significant role in their interaction with the surface. Furthermore, these dense biological interfaces are highly charged, with both steric and electrostatic contributions to NP stabilization. Despite the differences in the nature of binding, based upon the similar overall binding affinities and stabilization mechanisms for the two different ligand classes, comparable degrees of Au NP stability in colloidal suspensions are anticipated and observed.

DOI: 10.1021/acsami.5b01461
ACS Appl. Mater. Interfaces 2015, 7, 8843−8851

Reduction of 4-Nitrophenol. Once the Au nanomaterials were characterized for their morphological and optical properties, they were used as catalysts for the reduction of 4-nitrophenol. Because this reaction occurs directly on the metallic surface,[37] it provides insight into the structure and accessibility of the metal surface in solution. Additionally, the reaction is relatively quick and easily monitored using UV−vis absorbance changes from which apparent rate constants can be determined.[37] To probe their reactivity, each peptide-capped Au NP was employed in the reaction in water at temperatures ranging from 20 to 50 °C. To start the analysis, the NPs were first mixed with an excess of fresh $NaBH_4$ for 3.5 min, after which the 4-nitrophenol substrate was added to initiate the reaction. $NaBH_4$ is added to the reaction as a source of hydrogen atoms to saturate the metal surface and drive the reduction process.[36,37,40] Figure 4 presents the reaction analysis

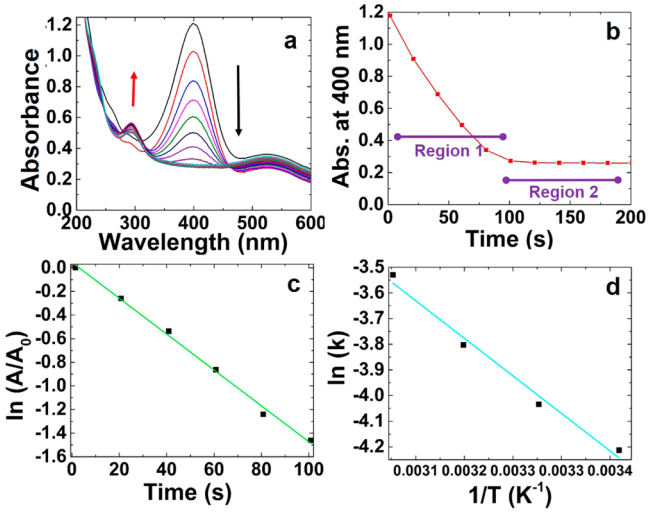

Figure 4. Determination of activation energies (E_a) for the 4-nitrophenol reduction reaction catalyzed by the peptide-capped Au NPs. For this example, the AuBP2-capped NPs reduced with $NaBH_4$ were used as the catalyst at 20 °C. Panel a shows the UV−vis spectra in which the peak at 400 nm corresponding to 4-nitrophenol decreases over time. Panel b displays the absorbance intensity at 400 nm as a function of time. Panel c presents the plot used to determine the pseudo-first-order rate constant, whereas panel d shows an Arrhenius plot from which the activation energy was determined.

for the Au NPs capped with AuBP2, which were reduced with $NaBH_4$. From the UV−vis analysis of Figure 4a, the successful reduction of 4-nitrophenol was visible by a decrease in absorbance at 400 nm along with the generation and growth of a new peak at 320 nm, corresponding to 4-aminophenol, the end product. In general, the reaction occurred rapidly with a decrease in the absorbance at 400 nm (Figure 4b, Region 1), followed by a steady baseline upon completion (Region 2) at time >100 s. Note that the peptides (AuBP1, AuBP2, and Pd4) alone did not exhibit any catalytic activity for the reduction of 4-nitrophenol at the time scales studied here (Supporting Information, Figure S5), demonstrating that the reactivity is catalyzed by the Au NP.

Because $NaBH_4$ was present in significant excess (100-fold), the reaction rate can be analyzed using pseudo-first-order kinetics.[37,42] Figure 4c presents this analysis in which absorbance (A) can be used in place of concentration, as previously shown.[37,42] The slope of this plot yields the apparent first-order rate constant, k.[37] To determine the activation energy (E_a) for each NP catalyst, an Arrhenius plot was generated from the rate constants at the selected reaction temperatures (Figure 4d). Such an analysis was conducted for all nine NP samples, prepared using the three different peptides in combination with the three different reductants. Figure 5

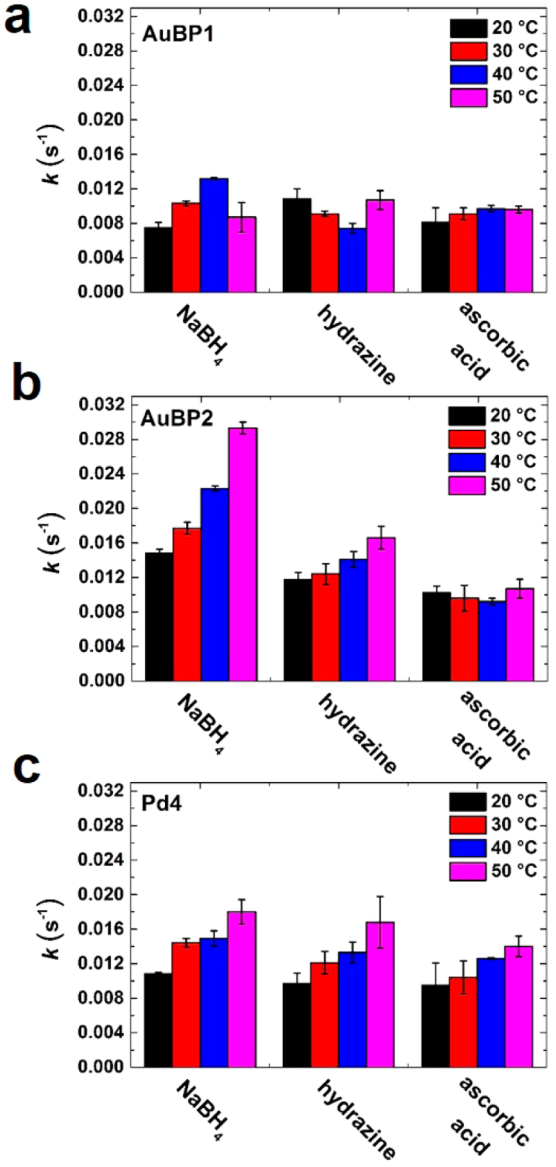

Figure 5. Comparison of the pseudo-first-order rate constants for the 4-nitrophenol reduction reaction for each of the peptide-capped Au NP catalysts prepared using the indicated reductants. (a) AuBP1-capped NPs; (b) AuBP2-capped NPs, and (c) Pd4-capped NPs.

presents an overall comparison of the rate constants as a function of reaction temperature, in which Figure 5a specifically presents the analysis for the particles capped with the AuBP1 sequence. For NPs produced using $NaBH_4$, the pseudo-first-order rate constant increased from 0.0075 ± 0.0006 at 20 °C to 0.0132 ± 0.0001 at 40 °C. However, at 50 °C, the rate constant actually decreased. This non-Arrhenius behavior was observed for all of the particles prepared using the AuBP1 peptide, regardless of the reductant used for NP synthesis. This suggests that the materials capped using this peptide are inherently

DOI: 10.1021/acsami.5b01461
ACS Appl. Mater. Interfaces 2015, 7, 8843−8851

unstable at elevated temperatures. As a result, their catalytic activity is also altered, leading to the observed non-Arrhenius temperature dependence. Such effects are consistent with previous studies of Au NPs capped with AuBP1.[23]

When the particles capped with the AuBP2 peptide were employed as catalysts, a monotonic increase in the rate constant with temperature was observed for particles reduced using $NaBH_4$ and hydrazine. For the $NaBH_4$ particles capped with AuBP2, the rate constants ranged from 0.0148 ± 0.0005 to 0.0293 ± 0.0007 s^{-1} from 20−50 °C, whereas for the AuBP2-stabilized particles reduced with hydrazine, the rate constants varied from 0.0124 ± 0.0012 to 0.0166 ± 0.0013 s^{-1} over the same temperature range. Interestingly, for the AuBP2-capped Au NPs generated using ascorbic acid, no significant change in the rate constant as a function of temperature was evident. For the Pd4-capped NPs, monotonic increases in rate constant with temperature were observed regardless of the reductant used to generate the NPs. Table 1 lists all of the E_a values that were

Table 1. Comparison of the Activation Energies for Each NP Catalyst

reductant	peptide name	particle size (nm)	E_a (kJ mol^{-1})
$NaBH_4$	AuBP1	3.2 ± 0.7	
	AuBP2	3.3 ± 0.7	26.2 ± 0.9
	Pd4	6.9 ± 2.6	18.1 ± 2.3
hydrazine	AuBP1	6.9 ± 2.1	
		19.7 ± 6.1	
	AuBP2	4.0 ± 0.9	15.4 ± 4.9
		14.2 ± 3.4	
	Pd4	4.1 ± 0.8	18.6 ± 2.4
ascorbic acid	AuBP1	53.3 ± 15.0	
	AuBP2	39.0 ± 18.8	
	Pd4	11.2 ± 6.4	15.6 ± 2.3

calculated for each of the NP systems, which ranged from 15.6 ± 2.3 for the Pd4-capped particles prepared using ascorbic acid to 26.2 ± 0.9 kJ/mol for the AuBP2-stabilized materials reduced using $NaBH_4$.

Differences in the catalytic activity observed between the different Au NPs can be attributed to two factors: NP stability during the reaction and the structure/morphology of the interface of the peptide-capped NPs. For the AuBP1-capped materials, regardless of the reductant used, and the AuBP2-capped materials reduced with ascorbic acid, the rate constants showed non-Arrhenius behavior, suggesting that the materials are not stable during the reaction. This is consistent with previous studies of the AuBP1-capped NPs, indicating that the peptides likely desorb from the particle surface and allow degradation or aggregation that produces a decrease in catalytic activity.[23] To confirm this instability, the Au NP spectrum before the catalytic reaction was started was compared with the spectrum at t = 12 min (red), at which time the reduction of 4-nitrophenol was complete (Supporting Information, Figure S6). As seen in these comparisons, a significant shifting and broadening of the LSPR band was observed for all materials for which non-Arrhenius behavior was noted. This broadening is indicative of aggregation of the Au NPs, strongly suggesting that the NP structure changes as a function of the reaction. For those materials that demonstrated Arrhenius behavior, no change in the LSPR of the Au NPs was noted, indicating no significant material structural changes due to the reaction. Unfortunately, due to the low Au NP concentration and high salt concentration of the reaction, TEM imaging of the materials after the reaction could not be completed. Conversely, when the AuBP2-peptide was used to cap the NPs, those structures prepared with $NaBH_4$ and hydrazine were quite reactive, but the rough surfaced materials prepared using ascorbic acid were again unstable. Interestingly, the E_a values for the AuBP2-capped particles varied significantly: 26.2 ± 0.9 kJ/mol for the materials reduced with $NaBH_4$ and 15.4 ± 4.9 kJ/mol for the hydrazine materials. Because the Au surface is the catalytic material, such changes likely reflect alterations in the surface structure, either through modifications based upon the biological molecules at the interface or through changes in the crystal morphology. Unfortunately, peptide-surface densities cannot be calculated due to the limited quantities of materials that can be prepared. Nevertheless, both effects are controlled via the peptide, which can alter crystal morphologies based upon its affinity for the metal surface. Finally, for the Pd4-passivated NPs, all of the materials were stable with rate constants that increased as a function of temperature. From this, three different activation energies were determined that were very similar in magnitude. This indicates that the catalytic surface structure of these materials is quite similar to allow easy access to the Au surface to drive the chemical process.

Recyclability studies of the NPs as catalysts for the reduction of 4-nitrophenol at 20 °C were also conducted with all nine peptide-capped Au NP systems. The resulting rate constants are shown in the Supporting Information, Figure S7. For this process, when the initial reaction period of 12 min was completed, fresh $NaBH_4$ and 4-nitrophenol were added to re-establish the initial reaction substrate concentration. In this manner, four reduction cycles were completed using the same materials. In general, the rate constants for all systems decreased slightly with consecutive cycles, as observed by slightly reduced k_{obs} values for cycles 2 and 3. Interestingly, an increase was noted in the rate constant for all NP systems in cycle 4. Previous studies have indicated that this increase could be due to the removal of the capping agent from the metal surface or the exposure of blocked catalytic structures after multiple reaction cycles.[36,48] Nevertheless, it is evident that the peptide-capped structures are highly reactive and maintain this reactivity after multiple catalytic cycles.

Direct comparison of the catalytic results for the bio-inspired materials of the present study to other Au NP systems for 4-nitrophenol reduction reaction can be completed to assess their reactivity. For example, Bhandari et al. studied the reaction using Au nanoparticle networks formed using the R5 peptide template (SSKKSGSYSGSKGSKRRIL) under similar conditions.[39] In that report, their measured E_a value was similar to that obtained here using the AuBP2-capped Au NPs (~29.0 kJ/mol for the Au nanoparticle networks versus 26.2 ± 0.9 kJ/mol for the AuBP2-based NPs). Further studies performed by Xia and co-workers examined the effects of changes in AuNP structure upon catalytic activity for 4-nitrophenol reduction.[38] They measured activation energies for this reaction catalyzed by Au nanocages, nanoboxes, and partially hollow nanoboxes, showing that the more open structures had higher catalytic activity, as reflected by activation energies of 28.04 ± 1.43 kJ/mol for the nanocages, 44.25 ± 2.62 kJ/mol for the nanoboxes, and 55.44 ± 3.15 kJ/mol for the partially hollow nanoboxes.[38] Interestingly, the E_a obtained using the nanocages is similar to the E_a measured here for AuBP2-capped NPs produced using $NaBH_4$, whereas the Pd4-capped NPs demonstrated even lower activation energies. This suggests that although the surface area

DOI: 10.1021/acsami.5b01461
ACS Appl. Mater. Interfaces 2015, 7, 8843−8851

plays a pivotal role in reduction activity, the type of capping ligand, corresponding effects on stability, and the degree of Au surface exposure are also key.

CONCLUSIONS

In conclusion, the results presented above indicate that both the materials-directing peptide and the reaction conditions work in concert to control the final morphology and surface state of peptide-capped NPs. Each peptide binds to the growing NP in solution, and thereby influences the particle size. This influence varies as a function of the binding strength and the number of anchor residues in the sequence. Furthermore, the number of nuclei formed immediately after reductant introduction varies as a function of the reductant strength. From this, the size of the materials can be directly controlled, a goal which generally remains challenging to achieve via bio-inspired approaches. An interesting rough surface morphology was observed using the weakest reductant, ascorbic acid, indicating that variations in the surface structure are possible. This was supported by changes in the catalytic efficiency of the materials for a reaction that is strictly dependent upon the NP surface. Taken together, these results present new avenues to access altered particle morphologies, sizes, and surface structures in a room-temperature peptide-mediated process via control of the reaction conditions and selection of the biological capping agent. Such effects could be important for the design of new NP systems for applications ranging from catalysis to biosensing and optics.

ASSOCIATED CONTENT

Supporting Information

Au NP particle sizing analysis histograms, SAED patterns for the peptide-capped Au NPs, analysis of AuBP1 and AuBP2 with Au and no reductant, calculated UV−vis spectra for AuBP1- and AuBP2-capped NPs, control 4-nitrophenol reduction studies conducted using the peptide only, UV−vis of the first and last spectra during the 4-nitrophenol reduction reaction, and k values obtained from recycling studies of 4-nitrophenol reduction at 20 °C. This material is available free of charge via the Internet at http://pubs.acs.org.

AUTHOR INFORMATION

Corresponding Author

*M. R. Knecht. Phone: (305) 284-9351. E-mail: knecht@miami.edu.

Author Contributions

The paper was written through contributions of all authors. All authors have given approval to the final version of the paper.

Funding

This work was supported by the Air Force Office of Scientific Research, grant FA9550-12-1-0226.

Notes

The authors declare no competing financial interest.

REFERENCES

(1) Briggs, B. D.; Knecht, M. R. Nanotechnology Meets Biology: Peptide-based Methods for the Fabrication of Functional Materials. *J. Phys. Chem. Lett.* **2012**, *3*, 405−418.

(2) Sarikaya, M.; Tamerler, C.; Jen, A. K.-Y.; Schulten, K.; Baneyx, F. Molecular Biomimetics: Nanotechnology through Biology. *Nat. Mater.* **2003**, *2*, 577−585.

(3) Han, M. S.; Lytton-Jean, A. K. R.; Oh, B.-K.; Heo, J.; Mirkin, C. A. Colorimetric Screening of DNA-Binding Molecules with Gold Nanoparticle Probes. *Angew. Chem., Int. Ed.* **2006**, *45*, 1807−1810.

(4) Huo, F.; Lytton-Jean, A. K. R.; Mirkin, C. A. Asymmetric Functionalization of Nanoparticles Based on Thermally Addressable DNA Interconnects. *Adv. Mater.* **2006**, *18*, 2304−2306.

(5) Nykypanchuk, D.; Maye, M. M.; van der Lelie, D.; Gang, O. DNA-Guided Crystallization of Colloidal Nanoparticles. *Nature* **2008**, *451*, 549−552.

(6) Maye, M. M.; Nykypanchuk, D.; van der Lelie, D.; Gang, O. A Simple Method for Kinetic Control of DNA-Induced Nanoparticle Assembly. *J. Am. Chem. Soc.* **2006**, *128*, 14020−14021.

(7) Lee, Y. J.; Yi, H.; Kim, W.-J.; Kang, K.; Yun, D. S.; Strano, M. S.; Ceder, G.; Belcher, A. M. Fabricating Genetically Engineered High-Power Lithium-Ion Batteries Using Multiple Virus Genes. *Science* **2009**, *324*, 1051−1055.

(8) Dickerson, M. B.; Jones, S. E.; Cai, Y.; Ahmad, G.; Naik, R. R.; Kröger, N.; Sandhage, K. H. Identification and Design of Peptides for the Rapid, High-Yield Formation of Nanoparticulate TiO_2 from Aqueous Solutions at Room Temperature. *Chem. Mater.* **2008**, *20*, 1578−1584.

(9) Pacardo, D. B.; Slocik, J. M.; Kirk, K. C.; Naik, R. R.; Knecht, M. R. Interrogating the Catalytic Mechanism of Nanoparticle Mediated Stille Coupling Reactions Employing Bio-inspired Pd Nanocatalysts. *Nanoscale* **2011**, *3*, 2194−2201.

(10) Coppage, R.; Slocik, J. M.; Briggs, B. D.; Frenkel, A. I.; Naik, R. R.; Knecht, M. R. Determining Peptide Sequence Effects That Control the Size, Structure, and Function of Nanoparticles. *ACS Nano* **2012**, *6*, 1625−1636.

(11) Hnilova, M.; Oren, E. E.; Seker, U. O. S.; Wilson, B. R.; Collino, S.; Evans, J. S.; Tamerler, C.; Sarikaya, M. Effect of Molecular Conformations on the Adsorption Behavior of Gold-Binding Peptides. *Langmuir* **2008**, *24*, 12440−12445.

(12) Slocik, J. M.; Govorov, A. O.; Naik, R. R. Plasmonic Circular Dichroism of Peptide-Functionalized Gold Nanoparticles. *Nano Lett.* **2011**, *11*, 701−705.

(13) Dickerson, M. B.; Sandhage, K. H.; Naik, R. R. Protein- and Peptide-Directed Syntheses of Inorganic Materials. *Chem. Rev.* **2008**, *108*, 4935−4978.

(14) Lévy, R.; Thanh, N. T. K.; Doty, R. C.; Hussain, I.; Nichols, R. J.; Schiffrin, D. J.; Brust, M.; Fernig, D. G. Rational and Combinatorial Design of Peptide Capping Ligands for Gold Nanoparticles. *J. Am. Chem. Soc.* **2004**, *126*, 10076−10084.

(15) Forbes, L. M.; Goodwin, A. P.; Cha, J. N. Tunable Size and Shape Control of Platinum Nanocrystals from a Single Peptide Sequence. *Chem. Mater.* **2010**, *22*, 6524−6528.

(16) Liang, M.; Deschaume, O.; Patwardhan, S. V.; Perry, C. C. Direct Evidence of ZnO Morphology Modification via the Selective Adsorption of ZnO-Binding Peptides. *J. Mater. Chem.* **2011**, *21*, 80−89.

(17) Flynn, C. E.; Mao, C.; Hayhurst, A.; Williams, J. L.; Georgiou, G.; Iverson, B.; Belcher, A. M. Synthesis and Organization of Nanoscale II-VI Semiconductor Materials Using Evolved Peptide Specificity and Viral Capsid Assembly. *J. Mater. Chem.* **2003**, *13*, 2414−2421.

(18) Banerjee, I. A.; Yu, L.; Matsui, H. Room-Temperature Wurtzite ZnS Nanocrystal Growth on Zn Finger-like Peptide Nanotubes by Controlling Their Unfolding Peptide Structures. *J. Am. Chem. Soc.* **2005**, *127*, 16002−16003.

(19) Tang, Z.; Palafox-Hernandez, J. P.; Law, W.-C.; Hughes, Z. E.; Swihart, M. T.; Prasad, P. N.; Knecht, M. R.; Walsh, T. R. Biomolecular Recognition Principles for Bionanocombinatorics: An Integrated Approach To Elucidate Enthalpic and Entropic Factors. *ACS Nano* **2013**, *7*, 9632−9646.

(20) Palafox-Hernandez, J. P.; Tang, Z.; Hughes, Z. E.; Li, Y.; Swihart, M. T.; Prasad, P. N.; Walsh, T. R.; Knecht, M. R. Comparative Study of Materials-Binding Peptide Interactions with Gold and Silver Surfaces and Nanostructures: A Thermodynamic Basis for Biological Selectivity of Inorganic Materials. *Chem. Mater.* **2014**, *26*, 4960−4969.

DOI: 10.1021/acsami.5b01461
ACS Appl. Mater. Interfaces 2015, 7, 8843−8851

(21) Saha, K.; Agasti, S. S.; Kim, C.; Li, X.; Rotello, V. M. Gold Nanoparticles in Chemical and Biological Sensing. *Chem. Rev.* **2012**, *112*, 2739−2779.
(22) Bhandari, R.; Coppage, R.; Knecht, M. R. Mimicking Nature's Strategies for the Design of Nanocatalysts. *Catal. Sci. Technol.* **2012**, *2*, 256−266.
(23) Li, Y.; Tang, Z.; Prasad, P. N.; Knecht, M. R.; Swihart, M. T. Peptide-mediated Synthesis of Gold Nanoparticles: Effects of Peptide Sequence and Nature of Binding on Physicochemical Properties. *Nanoscale* **2014**, *6*, 3165−3172.
(24) Hvolbæk, B.; Janssens, T. V. W.; Clausen, B. S.; Falsig, H.; Christensen, C. H.; Nørskov, J. K. Catalytic Activity of Au Nanoparticles. *Nano Today* **2007**, *2*, 14−18.
(25) Rosi, N. L.; Mirkin, C. A. Nanostructures in Biodiagnostics. *Chem. Rev.* **2005**, *105*, 1547−1562.
(26) Macfarlane, R. J.; Jones, M. R.; Lee, B.; Auyeung, E.; Mirkin, C. A. Topotactic Interconversion of Nanoparticle Superlattices. *Science* **2013**, *341*, 1222−1225.
(27) Lee, K.-S.; El-Sayed, M. A. Gold and Silver Nanoparticles in Sensing and Imaging: Sensitivity of Plasmon Response to Size, Shape, and Metal Composition. *J. Phys. Chem. B* **2006**, *110*, 19220−19225.
(28) Pandey, R. B.; Heinz, H.; Feng, J.; Farmer, B. L.; Slocik, J. M.; Drummy, L. F.; Naik, R. R. Adsorption of Peptides (A3, Flg, Pd2, Pd4) on Gold and Palladium Surfaces by a Coarse-Grained Monte Carlo Simulation. *Phys. Chem. Chem. Phys.* **2009**, *11*, 1989−2001.
(29) Brown, K. R.; Walter, D. G.; Natan, M. J. Seeding of Colloidal Au Nanoparticle Solutions. 2. Improved Control of Particle Size and Shape. *Chem. Mater.* **2000**, *12*, 306−313.
(30) Sau, T. K.; Murphy, C. J. Room Temperature, High-Yield Synthesis of Multiple Shapes of Gold Nanoparticles in Aqueous Solution. *J. Am. Chem. Soc.* **2004**, *126*, 8648−8649.
(31) Grzelczak, M.; Pérez-Juste, J.; Mulvaney, P.; Liz-Marzán, L. M. Shape Control in Gold Nanoparticle Synthesis. *Chem. Soc. Rev.* **2008**, *37*, 1783−1791.
(32) LaMer, V. K.; Dinegar, R. H. Theory, Production and Mechanism of Formation of Monodispersed Hydrosols. *J. Am. Chem. Soc.* **1950**, *72*, 4847−4854.
(33) Hostetler, M. J.; Wingate, J. E.; Zhong, C.-J.; Harris, J. E.; Vachet, R. W.; Clark, M. R.; Londono, J. D.; Green, S. J.; Stokes, J. J.; Wignall, G. D.; Glish, G. L.; Porter, M. D.; Evans, N. D.; Murray, R. W. Alkanethiolate Gold Cluster Molecules with Core Diameters from 1.5 to 5.2 nm: Core and Monolayer Properties as a Function of Core Size. *Langmuir* **1998**, *14*, 17−30.
(34) Coppage, R.; Slocik, J. M.; Briggs, B. D.; Frenkel, A. I.; Heinz, H.; Naik, R. R.; Knecht, M. R. Crystallographic Recognition Controls Peptide Binding for Bio-based Nanomaterials. *J. Am. Chem. Soc.* **2011**, *133*, 12346−12349.
(35) Pradhan, N.; Pal, A.; Pal, T. Silver Nanoparticle Catalyzed Reduction of Aromatic Nitro Compounds. *Colloid Surf. A* **2002**, *196*, 247−257.
(36) Saha, S.; Pal, A.; Kundu, S.; Basu, S.; Pal, T. Photochemical Green Synthesis of Calcium-Alginate-Stabilized Ag and Au Nanoparticles and Their Catalytic Application to 4-Nitrophenol Reduction. *Langmuir* **2010**, *26*, 2885−2893.
(37) Wunder, S.; Polzer, F.; Lu, Y.; Mei, Y.; Ballauff, M. Kinetic Analysis of Catalytic Reduction of 4-Nitrophenol by Metallic Nanoparticles Immobilized in Spherical Polyelectrolyte Brushes. *J. Phys. Chem. C* **2010**, *114*, 8814−8820.
(38) Zeng, J.; Zhang, Q.; Chen, J.; Xia, Y. A Comparison Study of the Catalytic Properties of Au-based Nanocages, Nanoboxes, and Nanoparticles. *Nano Lett.* **2010**, *10*, 30−35.
(39) Bhandari, R.; Knecht, M. R. Synthesis, Characterization, and Catalytic Application of Networked Au Nanostructures Fabricated Using Peptide Templates. *Catal. Sci. Technol.* **2012**, *2*, 1360−1366.
(40) Zhao, P.; Feng, X.; Huang, D.; Yang, G.; Astruc, D. Basic Concepts and Recent Advances in Nitrophenol Reduction by Gold- and Other Transition Metal Nanoparticles. *Coord. Chem. Rev.* **2015**, *287*, 114−136.
(41) Chan, W. C.; White, P. D. *Fmoc Solid Phase Peptide Synthesis: A Practical Approach*; Oxford University Press: New York, NY, 2000.
(42) Bhandari, R.; Knecht, M. R. Effects of the Material Structure on the Catalytic Activity of Peptide-Templated Pd Nanomaterials. *ACS Catal.* **2011**, *1*, 89−98.
(43) Coppage, R.; Slocik, J. M.; Ramezani-Dakhel, H.; Bedford, N. M.; Heinz, H.; Naik, R. R.; Knecht, M. R. Exploiting Localized Surface Binding Effects to Enhance the Catalytic Reactivity of Peptide-Capped Nanoparticles. *J. Am. Chem. Soc.* **2013**, *135*, 11048−11054.
(44) Cushing, B. L.; Kolesnichenko, V. L.; O'Connor, C. J. Recent Advances in the Liquid-Phase Syntheses of Inorganic Nanoparticles. *Chem. Rev.* **2004**, *104*, 3893−3946.
(45) Borsook, H.; Keighley, G. Oxidation-Reduction Potential of Ascorbic Acid (Vitamin C). *Proc. Natl. Acad. Sci. U. S. A.* **1933**, *19*, 875−878.
(46) Jana, N. R.; Gearheart, L.; Murphy, C. J. Evidence for Seed-Mediated Nucleation in the Chemical Reduction of Gold Salts to Gold Nanoparticles. *Chem. Mater.* **2001**, *13*, 2313−2322.
(47) Srisombat, L.; Jamison, A. C.; Lee, T. R. Stability: A Key Issue for Self-Assembled Monolayers on Gold as Thin-Film Coatings and Nanoparticle Protectants. *Colloid Surf., A* **2011**, *390*, 1−19.
(48) Shivhare, A.; Ambrose, S. J.; Zhang, H.; Purves, R. W.; Scott, R. W. J. Stable and Recyclable Au25 Clusters for the Reduction of 4-Nitrophenol. *Chem. Commun.* **2013**, *49*, 276−278.

DOI: 10.1021/acsami.5b01461
ACS Appl. Mater. Interfaces 2015, 7, 8843−8851